Radiative properties of micron-sized Al/air premixed flames described by an effective medium core-shell formulation

I. González de Arrieta, C. Blanchard, P. Laboureur, C. Chauveau, C. Genevois, O. Rozenbaum, F. Halter

This article was accepted by the International Journal of Heat and Mass Transfer on the 25th of December 2022 and made available online on the 4th of January 2023. The following document corresponds to the author version of the manuscript. The version of record can be accessed at https://doi.org/10.1016/j.ijheatmasstransfer.2022.123815.

Authors should cite the version of record as follows:

I. González de Arrieta, C. Blanchard, P. Laboureur, C. Chauveau, C. Genevois, O. Rozenbaum, F. Halter, Radiative properties of micron-sized Al/air premixed flames described by an effective medium core-shell formulation, International Journal of Heat and Mass Transfer 203 (2023) 123815.

Radiative properties of micron-sized Al/air premixed flames described by an effective medium core-shell formulation

I. González de Arrieta[a,b,*], C. Blanchard[a], P. Laboureur[c], C. Chauveau[c], C. Genevois[a], O. Rozenbaum[a], F. Halter[c]

[a] *CNRS, CEMHTI UPR3079, Univ. Orléans, F-45071 Orléans, France*
[b] *Physics Department, University of the Basque Country (UPV/EHU), E-48940 Leioa, Spain*
[c] *ICARE – CNRS, 1C Avenue de la Recherche Scientifique 45071 Orléans, France*

Abstract

The goal of this article is to contribute to the knowledge of the phenomenology of the poorly understood micron-sized Al/air flames, with the intention of assessing the viability of an energy carrier based on aluminum powders. To this end, the combustion efficiency, temperature, radiative profile, and solid combustion products of a flame prototype have been studied in depth. These fundamental parameters are required to explore the possibilities of recovering the energy released by these flames. In addition, a theoretical model has been established to analyze the radiative properties of the flame, derived for an optically thin collection of independent burning Al particles, each modeled by a core-shell geometry. The structure of the shell, made up of a cloud of alumina nanoparticles, has been modeled with an effective medium following the Maxwell-Garnett relation. This approach can reproduce the experimental results and is thus suggested as a starting point for modeling experiments characterized by strong emission by the nanoparticle cloud.

Keywords: aluminum combustion, alumina nanoparticles, emissivity, Lorenz-Mie scattering, effective medium approximations

1. Introduction

Aluminum combustion has been extensively investigated for decades, motivated by the role of aluminum powder as a component of solid rocket propellants

*Corresponding author.
Email address: inigo.gonzalez@cnrs-orleans.fr (I. González de Arrieta)

[1]. In recent years, it has also been proposed as a potential stand-alone green energy vector, given its high specific energy, wide availability, and the possibility of recycling the resulting aluminum oxide products using renewable energies [2, 3]. Unfortunately, the properties of Al/air two-phase flames are still poorly known compared to traditional hydrocarbon flames, with inconsistencies noted in the literature [4].

Aluminum combustion can proceed according to three modes depending on the Damköhler number (Da), which provides information on the competition between reaction kinetics and diffusion processes [5]. When the particle diameter is large enough ($Da \gg 1$), combustion takes place in the diffusive regime, typically characterized by vapor-phase combustion. This mode has been observed in many studies [6, 7], and various models have been proposed [8, 9]. Under these conditions, the adiabatic micro-flame temperature is estimated around 3540 K with the presence of species such as vaporized aluminum and gaseous aluminum sub-oxides that condense into nanometric Al_2O_3 particles. When the particle diameter is small enough ($Da \ll 1$), combustion is controlled by kinetics and usually takes place at the particle surface (heterogeneous combustion), forming an oxidized particle of equivalent size to the original particle. In this combustion mode, the combustion temperature must not exceed the vaporization temperature of aluminum, about 2790 K at 1 atm [5]. However, there are also instances of combustion processes that take place in the vapor phase but are kinetically limited [10]. The last option corresponds to the transition mode, which is a combination of the diffusion and kinetic controlled ones. For isolated particles with diameters smaller than 10 μm burning in air at atmospheric pressure, simulations have shown that a diffusion flame can only be self-sustaining by additional heat released from heterogeneous surface reactions [11, 12]. Thus, the combustion temperature is slightly higher than the vaporization temperature of aluminum and the combustion products are a mixture of nanometric and micrometric particles [5].

The intermediate $1 - 10$ μm range offers potential advantages for the development of combustion systems because of a promising balance between fast reaction rates and good energy content that are typical of nano- and macroparticles, respectively [13]. In this range, experimental determination of the

combustion mode and its properties is particularly important. In particular, the large difference between the typical flame temperatures of vapor-phase and kinetic-controlled modes, as well as the disparity in oxide particle sizes, has important consequences for the amount of thermal radiation emitted by the flame, which is crucial for pyrometry and combustion system sizing.

Metal combustion experiments are often characterized by a very large fraction of the total energy being released as thermal radiation from nanometric oxide particles [14]. Because of this, understanding the radiative properties of alumina clouds is crucial for successful modeling of the combustion processes detailed above. In the case of large individual particles, whose radiative profile can be directly imaged, numerical methods based on the radiative transfer equation are available [15]. However, for the more general case of a flame consisting of many burning particles, a phenomenological approach based on emission spectroscopy is often used. One solution consists of using approximations to derive a functional form of the emissivity, often as a power of the wavelength [16]. However, these approaches have been repeatedly called into question [4, 17]. Moreover, despite large efforts devoted to experiments on high-temperature alumina, its optical properties are still not well understood, as illustrated by the wide dispersion of absorption coefficient values reported in the literature [18]. Therefore, care must be taken when developing numerical models and choosing optical data sets to correctly describe the combustion problem with greater accuracy.

In this work, a micron-sized Al/air flame has been stabilized in the laboratory and the combustion mode has been analyzed by emission spectroscopy and particle residue analysis. A numerical model has been developed to relate the observed condensed-phase emission to phenomenological parameters describing the micro-flame geometry and optical properties of its constituents. The evaluation of the energy distribution between radiation and convection is crucial for energetic considerations.

2. Experimental setup

The experimental apparatus consists of a Bunsen type burner with an exit diameter of 32 mm, generating conical premixed metal flames in the open field.

Airflow controlled by a digital flowmeter sucks metal particles by Venturi effect which generates an aerosol in the burner main body. This one has a particular geometry of expansion and convergence to obtain a top-hat velocity profile at the burner exit with a homogeneous spatial distribution of the particles. An annular CH_4/air pilot flame of 180 W is left at the burner base in order to limit heat losses to the colder burner head and to reduce instabilities of the main Al/air flame. It is assumed that this pilot flame contributes to the main flame only thanks to the heat production, because the products of the methane/air combustion do not react with the aluminum particle as strongly as oxygen, and the gas expansion limit those products to mix with the fresh Al/air mixture. A detailed description of the experimental facility can be found in Ref. [13], while similar devices have also been described previously [10]. A sketch of the burner and its optical equipment is shown in Fig. 1.

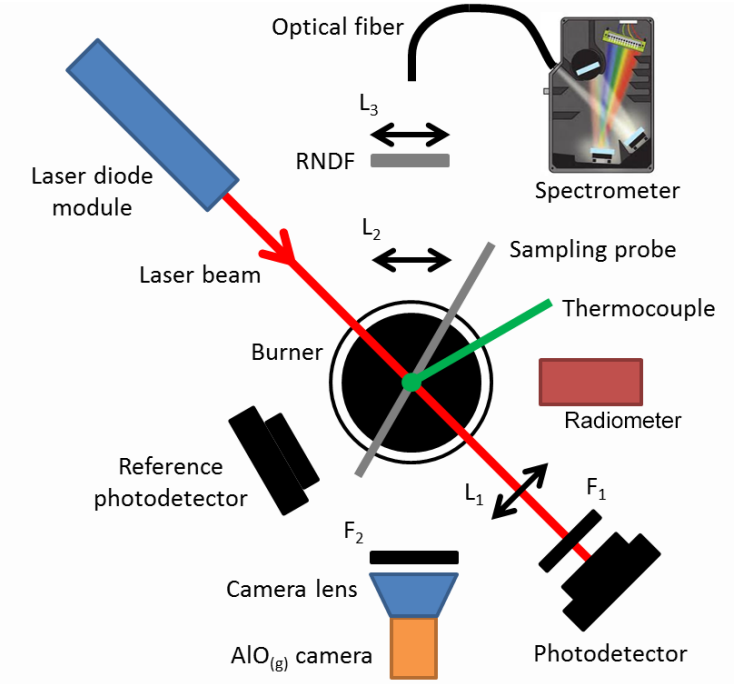

Figure 1: Sketch of the experimental facility. F_x: band-pass filters, RNDF: reflective neutral density filter, L_x: plano-convex lenses.

Aluminum powder was supplied by Poudres Hermillion and examined by scanning electron microscopy (SEM) coupled with an energy-dispersive X-ray spectroscopy (EDS) detector. A secondary-electron SEM image is given in

Fig. 2. The particles are mostly spherical, with a mass composition estimated by EDS at 99.8% Al, with the remainder corresponding to native alumina. A wide distribution of particle sizes is observed, which has been characterized at the burner exit by Fraunhofer diffraction using a HELOS Sympatec laser diffraction sensor (R5 optical module) during non-reactive tests. This distribution is detailed in Table 1, where d_x corresponds to the diameter for which x% of the particles are smaller. Large differences are noted between the particle size distributions in number and in volume. These data are consistent with images provided by SEM, indicating that there is no particle agglomeration between the tank and the burner outlet.

Table 1: Characteristic diameters of the Al particle distribution, expressed in terms of particle number or volume weighting.

	Number-weighted	Volume-weighted
d_{10} (μm)	0.92	1.77
d_{50} (μm)	2.63	7.58
d_{90} (μm)	4.32	29.38

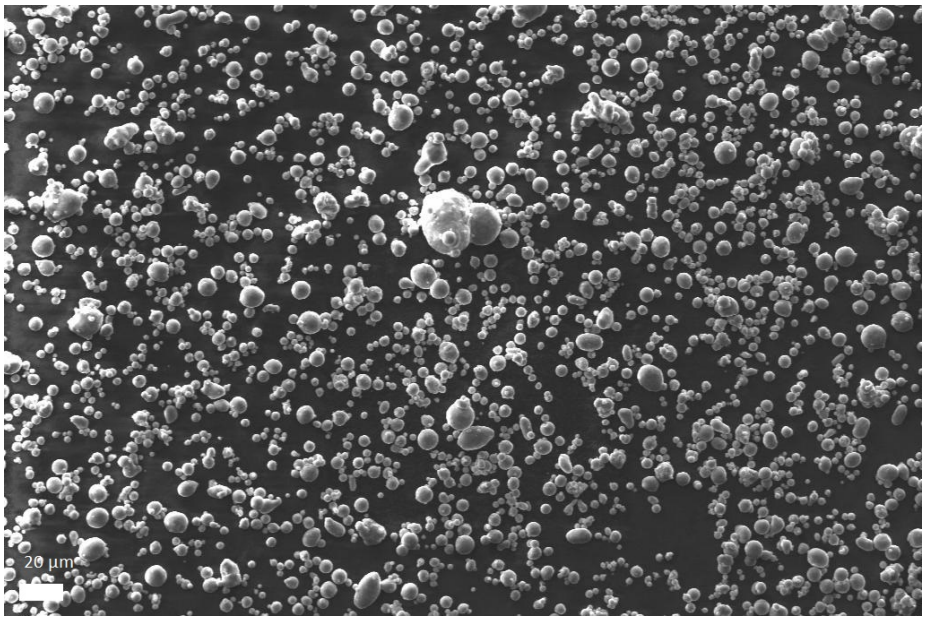

Figure 2: Secondary-electron SEM image of the aluminum powder. Scale bar: 20 μm.

In order to evaluate the concentration of the premixed flow (air/particles)

in real time at the burner exit, a set consisting of a laser diode module (central wavelength 670 nm), two biased Si photodetectors, a plano-convex lens (L_1, focal length 75.8 mm) and a band-pass filter (F_1, central wavelength 671 nm, FWHM 10 nm) has been set. As shown in Fig. 1, the laser beam passes through the flow at the burner center 2 mm above the burner outlet, between the burner head and the Al/air flame base. The laser beam is then focused to be measured by the photodetector equipped with the F_1 filter. The reference photodetector corrects the measured signal by subtracting the light emission generated by the Al/air flame over the filter bandwidth. The concentration is therefore estimated by laser attenuation using the Beer-Lambert method, where the extinction coefficient was determined experimentally in non-reactive tests.

Combustion is monitored by direct visualization thanks to a low-frequency camera (10 Hz, spatial resolution 20.9 pixels/mm, exposure time 10 μs) equipped with a band-pass filter (F_2, central wavelength 488 nm, FWHM 6 nm), highlighting the spatial distribution of the AlO(g) reaction intermediary and illustrating the flame geometry. In addition to Fig. 1, an optical assembly consisting of two plano-convex lenses (L_2, focal length 125 mm and L_3, focal length 53 mm), a UV reflective neutral density filter (optical density 2), an optical fiber (diameter 200 μm) and a spectrometer (Ocean Optics HR4000, linear CCD array) allows local spectral detection of the Al/air flame and a temperature determination using the emission of the AlO(g) reaction intermediate. The uncertainty of this procedure has been estimated from a maximal error of $\pm$180 K in previous tests, which can be converted into a standard uncertainty of $\pm$104 K. The study of the flame/plume radiation was performed with a tangential gradient radiometer having a viewing angle of 150° and operating at wavelengths between 0.3 μm and 20 μm. This differential sensor measures only the radiated power per unit area by subtracting the convective flux from the total value. The uncertainty of this measurement is based on a combination of the intrinsic uncertainty of the sensor and other sources related to the measurement method. For the radiant powers measured in this paper, the intrinsic uncertainty corresponds to $\pm$0.2 kW, whereas the combined standard uncertainty is estimated as $\pm$0.5 kW.

Finally, the solid combustion products were sampled and analyzed by transmission electron microscopy (TEM) and SEM coupled to an EDS probe to obtain

compositional and morphological information on the combustion products. The particles were dispersed first in ethanol and then a drop of the mixture was loaded on a copper grid layered by an amorphous holey carbon film.

3. Results

The structure of the flame can be seen in Fig. 3 for an Al/air equivalence ratio $\Phi = 0.95$. This corresponds to a global equivalence ratio obtained by considering the total flow rates of injected aluminum and air. The reaction zone, where most of the emitted radiation is generated, is observed through the F_2 filter bandwidth. The flame is conical with a flame tip not exceeding 40 mm above the burner outlet, consistent with other burners [16]. The flame structure is consistent with a point source approximation, as the reaction zone is much brighter than the plume.

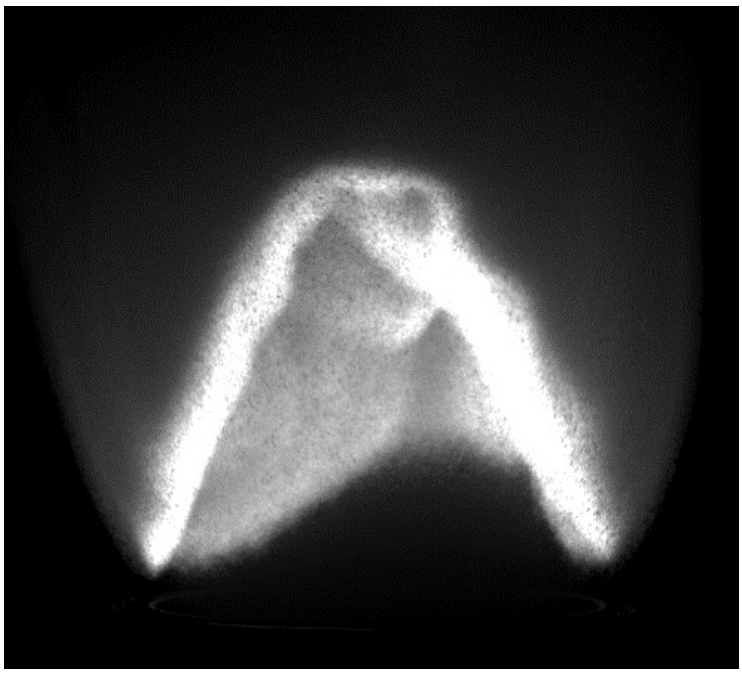

Figure 3: Image of the reaction zone through the bandwidth of the main AlO(g) emission. Burner exit diameter: 32 mm.

According to the data in Table 1, more than half of the injected particles have diameters smaller than 3 μm; thus, they would be expected to react in a heterogeneous regime when studied in isolation. This mode would be revealed by a

flame temperature not exceeding 2790 K and micrometric combustion products. However, because of the wide size distribution of the powder and the possibility of group effects, the combustion mode must be determined experimentally by emission spectroscopy and morphological characterization of the condensed residue. Following the methodology described in [13], a dimensionless emission spectrum of the reaction zone is shown in Fig. 4 for an Al/air flame with an equivalence ratio of 0.95. It consists of both a continuous background emission due to the thermal radiation of the condensed phase and the emission of gaseous species by the rotational-vibrational transitions of the electronic levels. AlO(g) emissions in the system $B^2\Sigma^+ \rightarrow X^2\Sigma^+$ (blue-green) are predominant, while Al(g) emissions can be observed at 394.4 nm and 396.1 nm. Lines corresponding to Na and Li (not shown) are also present. The gas temperature can be determined by fitting the AlO(g) bands, and is revealed to be constant around 3150 K for Al/air equivalence ratios ranging from 0.6 to 1.3 [13]. This temperature within the reaction zone is 350 K higher than the boiling temperature of aluminum. Therefore, the results suggest that particles burn in a vapor-phase mode controlled more by diffusion than kinetics, although the transition mode cannot be completely excluded.

The study of condensed combustion products makes it possible to validate the general mechanism of aluminum oxidation. For an equivalence ratio of 0.95, the condensed combustion products were collected by agglomeration on a metal rod in the plume 90 mm above the burner outlet, assuming all particle sizes have the same sticking ability. This sample was analyzed by electron microscopy, as shown in Fig. 5. Although some micrometric spherical particles with diameters between 1 μm and 7 μm are found, the vast majority of the combustion products consist of nanometric particles. The sphericity of the larger particles indicates that they are formed in the liquid state during the combustion process, and they probably correspond to the molten alumina lobe residue present in the larger particles during vapor phase combustion. The amount of micrometric combustion products is in accordance with the initial alumina volume of the passive layer covering the largest aluminum particles. In contrast, the nanoparticles were analyzed by TEM coupled with an EDS probe, as shown in Fig. 5 (bottom). Nanoscale products are spherical and follow a log-normal size

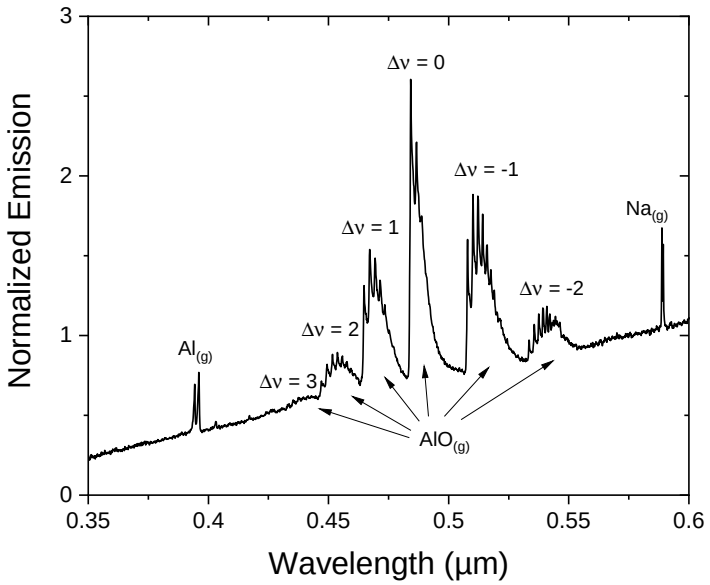

Figure 4: Dimensionless emission spectrum for an equivalence ratio of 0.95, evidencing the vapor-phase nature of this combustion process. The spectrum has been normalized to the value at 0.58 μm.

distribution with a mode at a radius of 65 nm. The particles are independent and an ethanol bath during sample preparation is sufficient to separate them.

EDS analyses of the nanometric products show that they are only composed of alumina, but traces of nitrogen have been found in the micrometric particles, especially around darker areas in the surface. This observation may be consistent with the hypothesis of NO retro diffusion to the aluminum droplet surface and its surface reaction [19]. Nevertheless, the absence of significant amounts of nitrides inside these micrometric particles indicates that reactions with nitrogenated gaseous species are very weak and confirm that the major oxidation mechanism of aluminum is its transformation into alumina. In addition, the absence of aluminum residue suggests that the combustion efficiency is close to unity under our experimental conditions.

The analysis of the combustion products suggests that all particles burn in the vapor phase. The difference with the heterogeneous mode, which is more representative of micron-sized particles when burning in isolation, may lie in the group effect and the modification of boundary conditions. Radiative heat

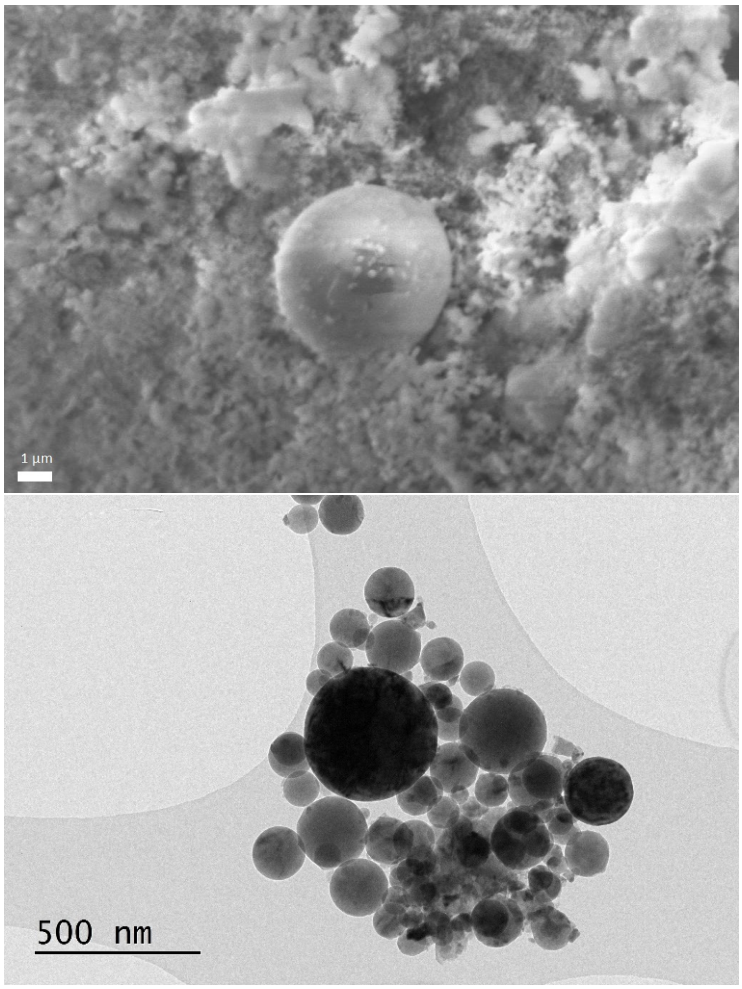

Figure 5: Top: SEM image of the combustion products, featuring a large micrometric particle surrounded by nanometric residue (scale bar: 1 μm). Bottom: bright-field TEM image of the nanoscale condensed combustion products.

transfer is sometimes suggested as a mechanism for group effects, but this has been contested [20]. Instead, gas transport probably plays a bigger role in affecting boundary conditions, especially in a very heterogeneous powder. The biggest particles burn in diffusion mode and can help the smaller particles (which are most sensitive to environmental conditions [5]) burn in this same mode by heating the gas around them. Indeed, the vapor-phase combustion mode has been observed in the context of the combustion of only slightly larger aluminum particles [21].

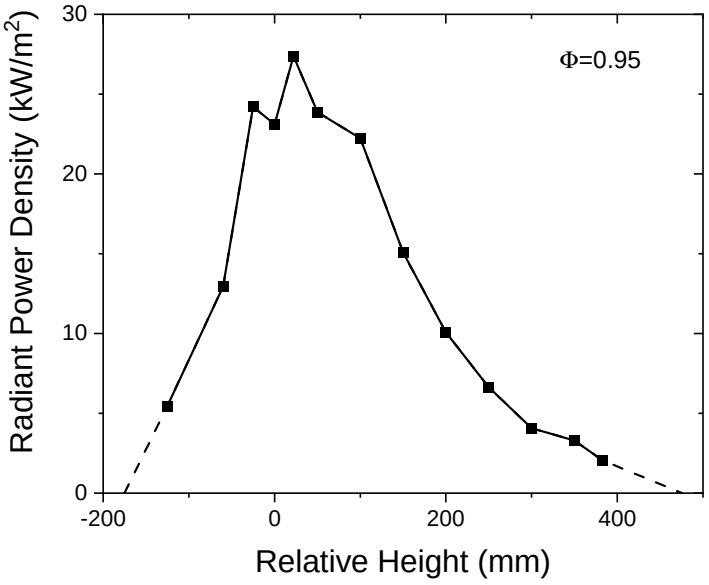

Figure 6: Axial profile of the radiant power density for a $\Phi = 0.95$ Al/air equivalence ratio, including linear extrapolations to zero at both ends of the measured range.

Finally, the extreme brightness of the Al/air flame motivated a study of its energy release by radiation. An axial radiometer was used to evaluate the energy radiated by the flame and the plume to compare it to the total energy released by aluminum oxidation. This information is important as a sizing parameter in the thermal design of combustion systems. The study of the total radiation emitted by the flame was carried out using radiant power measurements perpendicular to the burner axis at different heights using a radiometer previously described. The radial coordinate of the radiometer is kept constant at 135 mm from the burner center for all vertical positions. The distribution of radiant power density,

as a function of height relative to the burner exit, is shown in Fig. 6. The maximum radiation is obtained at the reaction zone, as expected. The method of determining the total radiant power is the same as for traditional burner flames [22], consisting of integrating the axial profile on an imaginary cylindrical surface. The high reflectivity of the brass burner suggests that most radiation emitted through the bottom of the imaginary cylinder finds its way back to the sides, whereas the emission from the top surface is considered negligible. The total radiant power obtained by this method for a flame with 0.95 Al/air equivalence was $P_e = 5.9 \pm 0.5$ kW, corresponding to 78% of the estimated total power release of 7.6 kW, calculated assuming a full oxidation of the injected aluminum. An Al mass flow of 0.25 g/s and a residence time of 6 ms in the reaction zone were used for estimating this quantity. This value will be tested against the model predictions in the following section. It must be noted that this extraordinary radiative fraction stems from the very high temperatures (3150 K) of the reaction zone. In comparison, it has been shown that the radiated portion released by the combustion of a single magnesium particle, with much lower oxide boiling point, is about 40% [14].

4. Numerical simulations

4.1. Theoretical model

Direct simulation of the electromagnetic problem of diffusion-controlled flames is complicated by the large number of nanometric oxide particles that surround each burning Al particle. This high computational demand can be reduced by adopting a number of simplifications. First, only the condensed phases in the reaction zone are assumed to take part in thermal emission, modeled as an optically thin collection of independent micro-flames. The optically thin approximation is motivated by the small size of the burner and the relatively low concentration of Al particles. Secondly, the dispersion of sizes is approximated by a single representative size for the Al particles, which has been chosen as the volume-average median diameter of 7.58 μm (Table 1). The use of volume averaging is motivated by the fact that this scaling law is representative of transitional flames, for which a defined flame front is not well formed, a situation that is more typical of smaller particles when burning in the vapor phase

[4]. Burning particles in this regime thus behave as semi-transparent materials, rather than as surface emitters. Thirdly, an effective medium approximation is used, where the oxide particle cloud is homogenized as a solid shell surrounding an Al core. This geometry can be solved even in the non-isothermal case using Lorenz-Mie calculations making use of the model by Mackowski and coauthors, developed and tested for coal particles surrounded by soot clouds [23, 24]. The main steps of the model are summarized in Fig. 7. The presence of oxide caps in the larger particles has not been considered in this model, as their potential contribution was deemed negligible.

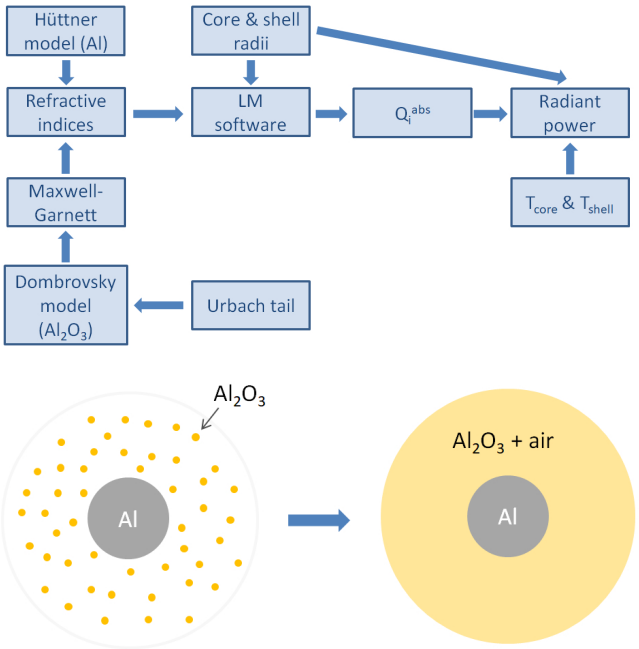

Figure 7: Top: conceptual scheme representing the steps in the theoretical model. Note that temperatures also implicitly affect the values of the refractive indices. Bottom: conceptual idealization of the micro-flame geometry, consisting of identical core-shell particles with shells that are homogenized using an effective medium approximation.

A crucial aspect of this theoretical model is the concept of homogenization. Effective medium theories are useful approximations to the properties of a composite, provided that the scale of the inhomogeneities is much lower than the measurement scale. For the particular case of independent (i.e., non-percolating) particles, the well-known Maxwell-Garnett model can be used [25].

In the case of optically soft composites, for which the refractive indices of both phases are close in magnitude, the allowed variability in the effective optical constants is heavily restricted by the Hashin-Shtrikman bounds [26]. Moreover, this approach has been validated for relatively large core sizes by comparison to a direct calculation using the radiative transfer equation [23]. It has also been used to study the influence of radial thermal gradients and phase transitions on the radiative properties of alumina particles [27]. The model is based on the following expression for the radiance emitted by a multi-layer particle (in the particular case of two layers):

$$L = Q_s^{abs} L_{bb}(T_s) + \left(\frac{r_c}{r_s}\right)^2 Q_c^{abs} L_{bb}(T_c), \tag{1}$$

where L stands for the spectral radiance of the core-shell system (W sr^{-1} m^{-2} μm^{-1}), L_{bb} for blackbody radiance as given by Planck's law, Q_i^{abs} for the absorption efficiency, r_i for the external radius of each layer (c: core; s: shell), and T_i for its temperature.

The biggest uncertainty in the simulation is the choice of a refractive index parameterization. The optical indices of Al have been obtained from the phenomenological Hüttner model [28], but notable disagreements are found between different sources of optical data on liquid alumina [18]. A broad classification can be made between data based on measurements of alumina samples heated up to the melt, and those obtained by combustion of aluminum. Data belonging to the latter group show consistently higher values of the absorption index around visible wavelengths, while the difference is generally lower in the infrared. Still, there are many variables that can drastically alter the absorption coefficient, such as pressure or the oxygen content of the atmosphere [29, 30]. Two of the most widely used models are those given by Dombrovksy [31, 32], and Parry and Brewster [33]. The former model is based on a temperature extrapolation of experimental data from two sources [34, 35], while the latter is a parameterization of combustion experiments performed by the same authors. The best agreement was found with the Dombrovsky model, whose expressions for the real and imaginary parts of the complex refractive index $\tilde{n} = n + ik$ are reproduced below:

Table 2: Best-fit values for the parameters of the optical model, within the limits described in the text. The temperature and size of the Al core were not allowed to vary. The optical gap energy can be converted to a wavelength value making use of the equivalence E [eV] $= 1.24/\lambda$ [μm].

T_c (K)	T_s (K)	d_c (μm)	d_s/d_c	f	E_{op} (eV)	b (μm^{-1})	c (μm K)	N_{part}
2743	3206	7.58	3.1	0.3	3.71	0.1285	13810	$2.43 \cdot 10^6$

$$n_0^2(\lambda) - 1 = \frac{1.024\lambda^2}{\lambda^2 - 0.003776} + \frac{1.058\lambda^2}{\lambda^2 - 0.01225} + \frac{5.281\lambda^2}{\lambda^2 - 321.4}, \tag{2}$$

$$n(\lambda, T) = n_0(\lambda)[1 + 2.02 \cdot 10^{-5}(T - 473)], \tag{3}$$

$$k(\lambda, T) = 0.002(1 + 0.7\lambda + 0.06\lambda^2) \cdot \exp[1.847 \cdot 10^{-3}(T - 2950)], \tag{4}$$

where λ is the wavelength in μm and T is the temperature in K.

4.2. Numerical results

Numerical implementation of the model relies on calculating the absorption cross sections corresponding to the core-shell geometry is shown in Fig. 7. The model can be implemented using any software capable of computing solutions to the Lorenz-Mie theory, whose extension to coated spheres is well known. These calculations were performed for 100 wavelengths from 0.4 to 5 μm using bins of equal energy width, to avoid undersampling in the short-wavelength range. The number of required multipolar expansion degrees was explored in the classic reference by Wiscombe [36]. For the purposes of this paper, it was found to be approximately proportional to the size parameter corresponding to the external radius of the core-shell ($x = 2\pi r_s/\lambda$). Therefore, an adaptive scheme was adopted, in which each wavelength was computed using a proportional number of terms. A number of degrees $N = 1.2x$ was found to converge to the required precision in the calculated absorption cross-sections. Limiting the number of degrees to the minimum that ensured convergence is important to limit the calculation time for non-linear least-squares fitting of the data.

The parameters of the numerical simulations (Table 2) were varied to fit the continuum emission revealed by emission spectroscopy. Several constraints

allowed a simplification of the fitting procedure, such as fixing the temperature of the core to be the Al boiling point (2743 K). Besides, the ratio between the external and internal diameters at atmospheric pressure was observed to be between 3 and 3.5 in studies on individual particles of larger size [37]. Calculations were attempted with the Parry-Brewster and Dombrovsky models (Fig. 8) Good agreement to experiment was obtained for the Dombrovsky model in the $0.55 - 0.7$ μm spectral range, whereas the Parry-Brewster model was unsatisfactory at both extremes of the measured spectrum. However, even for the Dombrovsky model, the calculated emission decreased rapidly in the blue end of the spectrum, a deficiency which could not be compensated adequately by parameter variation. This motivated the consideration of an inaccuracy in the optical model, and the introduction of an additional term to account for the pre-band gap absorption, known in solid-state physics as the Urbach tail.

Pre-gap absorption is well established to occur in liquid alumina, although it depends heavily on factors such as the oxygen partial pressure [30]. The contribution of the Urbach tail to the extinction index of alumina was modeled using the appropriate component of the analytical model by Plastinin *et al.* [38]:

$$k_u = b\lambda \exp\left(\frac{c}{T}\left(\frac{1}{\lambda} - \frac{1}{\lambda_{op}}\right)\right), \tag{5}$$

where b and c are free parameters to determine the strength of the phenomenon, and λ_{op} corresponds to the optical gap wavelength in μm.

The free parameters have been varied to improve the fitting to the experimental results, and values distinct from those reported in the original work have been found. In the case of the energy gap, only wavelength values corresponding to energies in $3.6 - 4$ eV range reported in the literature have been considered [39, 40], leading to a best value of 0.334 μm or 3.71 eV. Besides, the original model considers the optical band-gap wavelength λ_{op} to be dependent on temperature, but the changes are excessive for the temperature range under consideration. The comparison between the extinction index of the Dombrovsky model and that considering the Urbach tail is shown in Fig. 9. The Parry-Brewster model is also illustrated for completeness. Contrary to this latter case, for which a very broad UV-VIS absorption was reported [33], the Urbach absorption mechanism introduced in the Dombrovsky model does not

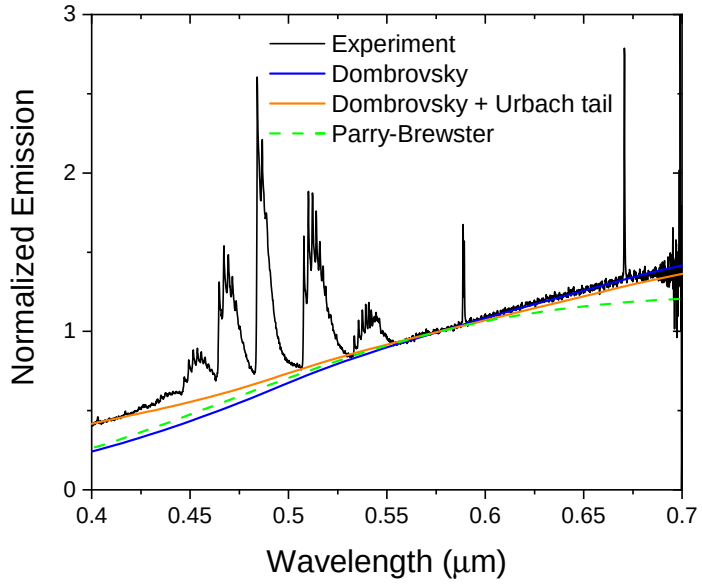

Figure 8: Experimental and simulated emission spectra, normalized to the value at 0.58 μm. Results corresponding to simulations using the Dombrovsky and Parry-Brewster are compared, as well as those corresponding to the Urbach tail extension to the Dombrovsky model.

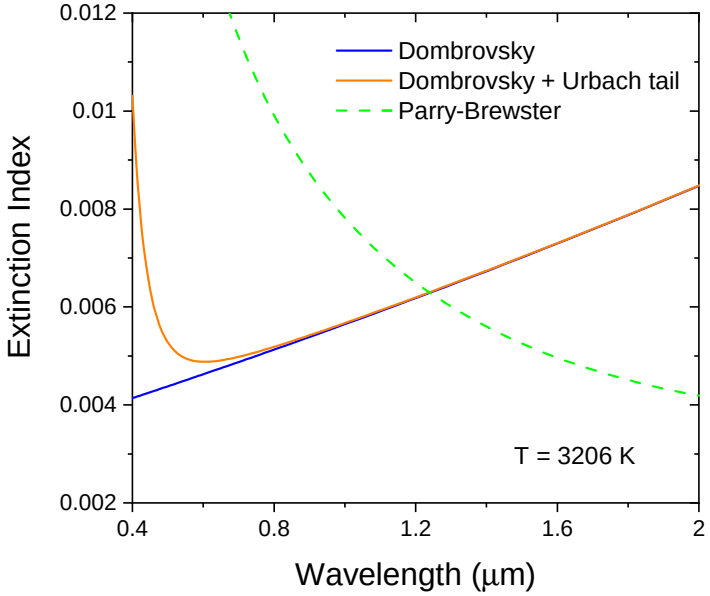

Figure 9: Extinction index k of the optical models used to generate the data shown in Fig. 8.

extend beyond the visible range, with a sharp onset around 0.6 μm. It is important to note that the introduction of this term is perfectly compatible with the data on which the Dombrovsky model is based, which only reaches wavelengths down to 0.63 μm [34].

The total power emitted by the flame is obtained from the Al particle feed rate and the residence time in the reaction zone. The spectral distribution of this radiant power $P_{e,\lambda}$ can be seen in Fig. 10, where the contributions from the Al core and Al_2O_3 shell are shown independently. The contribution from the metal is clearly negligible for practical purposes, especially in the visible range. This stems from both its lower temperature and size. The contribution from the shell has a heavily distorted blackbody shape, corresponding to an emissivity that changes significantly with wavelength. The total power is obtained by multiplying the radiance L emitted by one microflame/burning particle (Eq. 1) by its geometric cross section πr_s^2, the hemispherical solid angle, and the number of particles in the reaction zone (estimated from the mass flow, residence time, and assumed size of $d_c = 7.58$ μm) [41]:

$$P_e = N_{part} 4\pi (\pi r_s^2) L. \tag{6}$$

The total radiant power is obtained by integration of the spectral values shown in Fig. 10 in the $0.3 - 5$ μm range, to match the spectral range measured by the radiometer. All radiation emitted above 5 μm was considered negligible, while the $0.3 - 0.4$ μm range was estimated by linear extrapolation. The total radiant power was found to be 5.94 kW, in excellent agreement with the experimental value of 5.9 ± 0.5 kW. The radiative contribution from the 0.18 kW methane pilot flame is negligible. However, it must be noted that the model did not take into consideration certain factors, such as gas radiation or the presence of colder particles with reduced emission, which are known to be potential sources of emitted profile distortion [42]. It is possible that these systematic effects cancel each other out. The model also does not take into account effects such as self-absorption or scattering of the radiation emitted by the microflames, phenomena which would be required for the description of optically thicker systems. Nevertheless, the extent of the agreement between the theoretical and experimental values serves as an important validation step

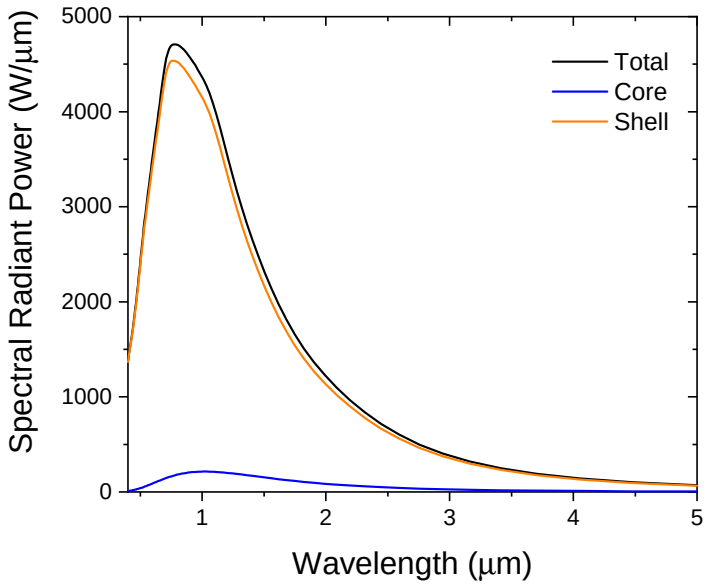

Figure 10: Spectral radiant power emitted by the condensed phases of the flame, divided into core and shell contributions. The Dombrovsky model at 3206 K with the Urbach tail addition has been used.

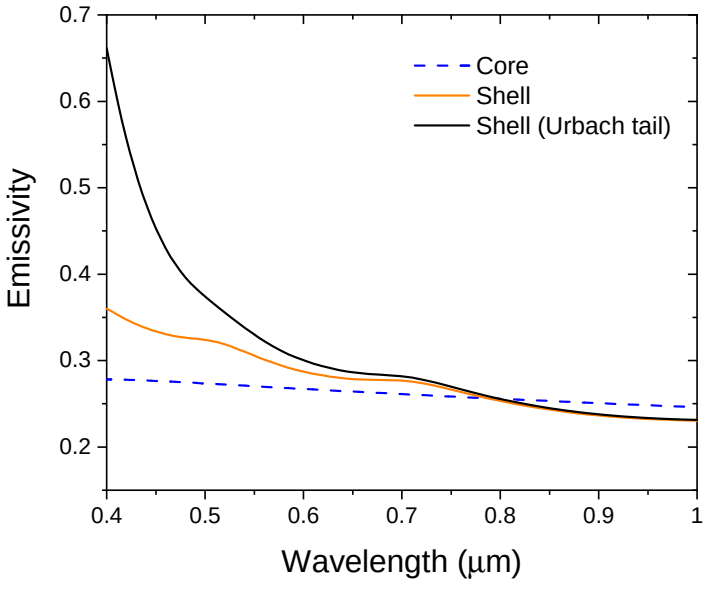

Figure 11: Emissivities of the Al core and the Al_2O_3/air shell, with and without considering the effect of the Urbach tail.

of the model. By contrast, the much higher extinction index associated to the Parry-Brewster model (as seen in Fig. 9) leads to a much higher value of 7.24 kW, in significantly poorer agreement.

The small contribution of the core to the total radiant power allows considering the problem as approximately isothermal, thus enabling thermographic studies of the flame by considering exclusively the spectral dependence of the alumina cloud emissivity. This is explored in Fig. 11, where the absorption efficiency Q^{abs} of the core and the shell are plotted as a function of wavelength in the visible range. The equivalence between this property and the emissivity of a small particle is well established [41]. It must be noted that the emissivities of particles are not independent of their size or, in the case of the shell, the alumina filling factor. This means that literature values of this property cannot be directly compared. Finally, fitting the emissivity to a power law of the type $A\lambda^n$ in the $0.6 - 0.8$ μm range reveals an exponent of $n = -0.37 \pm 0.03$ for the solution neglecting the Urbach tail and -0.49 ± 0.03 when considering this contribution.

5. Discussion

From a practical standpoint, this calculation procedure allows estimating realistic exponents for pyrometric applications. The fitting of the emissivity to a power law in the relevant range between 0.6 and 0.8 μm gives an exponent far from usually assumed values, such as -2 and -1. It must be noted that fitting both emissivity curves to power laws in extended spectral ranges led to unsatisfactory fittings, with the stated power laws being of use only in a restrictive range that is practical for applications. The unsuitability of general power laws is particularly relevant for studies which derive the temperature of the solid phase by fitting in the entire visible range [16]. Moreover, the typically assumed λ^{-2} power-law dependence of the emissivity of alumina is based not only on the Rayleigh approximation, but also on the Parry-Brewster model [17]. Therefore, general power laws such as λ^{-1} and λ^{-2} are heavily contingent on the specifics of the problem, and should not be trusted *a priori*, even if they find success in particular applications [16]. Besides, the specific nature of emission spectroscopy of condensed phases, which often leads to broad and featureless

curves, means that even goodness of fit is not necessarily an appropriate criterion, as slight differences can lead to widely diverging temperature estimations [4]. Finally, it is worth noting that the Rayleigh approximation, while applicable to very small nanoparticles, loses its predictive power to describe a situation like the one described in this work, consisting of large and dense ensembles of such particles.

Regarding the optical properties of alumina, the use of the Dombrovsky model should not be interpreted as a validation of the suitability of this model in general. This is clear by the fact that an amendment had to be made at short wavelengths. Furthermore, it is well known that this model does not consider the reduction in density after melting, which significantly lowers the real part of the refractive index [33]. However, the emissivity in semitransparent materials is most crucially dependent on the imaginary part of the refractive index [29]. The most important conclusion that can be extracted from this choice of refractive index model is that no single model can be trusted *a priori* to describe the emission of liquid alumina in a particular set of circumstances. Indeed, even the Urbach tail extension, which was based on the Plastinin model [38], required important modifications to the parameter values to fit the results shown in this work. Moreover, it is worth noting that, in contrast with the conclusions of Ref. [18], a model based on results obtained for molten alumina [34] is more representative of the results in this work than one based on combustion experiments [33]. The sensitivity of the results to the choice of extinction index means that uncritical use of optical models can lead to important inaccuracies. Thus, validation procedures for the optical parameters should be included in the simulations whenever possible.

A crucial step in the formulation of the approximations has been the assumption that the absorption cross-section of the nanoparticle ensemble can be modeled as an effective medium. The particular choice of the Maxwell-Garnett (MG) model is motivated by the tightness of the Hashin-Shtrikman bounds for an alumina/air composite [26]. Any effective medium approximation gives similar results for a composite satisfying the condition that the complex refractive index of the particles is not significantly different from that of the matrix ($|\tilde{n} - 1| < 1$ for particles in air). Therefore, the MG model was chosen for its

topological similarity to the sample (ensemble of separate spheres) and its simplicity. However, the non-negligible size of the nanoparticles compared to the lowest wavelengths under study requires a more rigorous proof of the suitability of the EMA approach itself, regardless of the particular model used. It is not the aim of this calculation to suggest that the MG mixing rule is valid in general, or in an unrestricted sense. It is well known that deviations from the predictions by effective medium approximations can take place even for sub-wavelength particles, if the optical indices correspond to resonant behavior [43]. The goal of this method is to prove that, for the rather restrictive circumstances that characterize this work, the MG rule can be used to provide a sufficiently accurate value of the absorption cross-section of an ensemble of particles that is denser than the filling factors usually considered.

Theoretical simulation of combustion processes is notoriously complex, and the simplified method presented in this work does not attempt to describe the radiative properties of Al/air flames in general. Nevertheless, this framework makes it possible to describe some combustion processes by considering only a reduced number of parameters, together with an optical model for the Al_2O_3 complex refractive index. The calculation has been kept deliberately simple, in order to illustrate how this choice of parameters is able to reproduce the observed data and to provide useful conclusions and predictions. Despite the good agreement between the experiment and the data, the accuracy of some of the approximations needs to be tested in more detail. However, a more in-depth study of the radiation component of Al/air radiation problems requires a more sophisticated approach, which can nevertheless be built upon this framework.

6. Conclusions

An experimental device capable of stabilizing conical Al/air premixed flames with micrometric particles has been described. Even the smallest particles in this setup seem to burn in the vapor-phase combustion mode, as evidenced by emission spectroscopy and analysis of the combustion products. The combustion efficiency is close to unity, with radiation contributing almost 80% of the total heat release. This significant amount of radiation is a crucial parameter for the design of systems to extract energy from these flames. A model based on

the assumption of independent emission by effective particles has been shown to be useful. This allows calculating the emission of the flame in an optically thin regime, by modeling each microflame as a core-shell electromagnetic problem, where the Al_2O_3 particle cloud is homogenized using the Maxwell-Garnett effective medium approximation. This phenomenological model can be implemented and generalized easily by any program capable of computing Lorenz-Mie solutions. The availability of a model is useful to estimate the accuracy of two-color pyrometry, as well as to correct multispectral pyrometry. Future work needs to be carried out to implement this method as an inverse problem to extract optical data of the particles, as well as in thermographic studies and thermal design. Moreover, direct simulations of the electromagnetic interaction between the alumina particles will be carried out to move beyond the Maxwell-Garnett approximation. Finally, phenomena such as self-absorption and scattering will have to be considered when adapting the model to optically thicker flames, such as those corresponding to larger burners or at more fuel-rich conditions.

Acknowledgments

This work is part of the OUTWARDS (ID: ANR 19-CE05-0021) and STELLAR (ANR-18-CE05-0040) projects, funded by the Agence Nationale de la Recherche (ANR). I. González de Arrieta acknowledges support from the Basque Government by means of a post-doctoral fellowship (POS-2021-2-0022) and thanks Timothée Guerra for help with programming. The authors acknowledge the ICMN laboratory (Orléans, France) for access to the TEM.

References

[1] C. Griego, N. Yilmaz, A. Atmanli, Analysis of aluminum particle combustion in a downward burning solid rocket propellant, Fuel 237 (2019) 405–412.

[2] J. M. Bergthorson, S. Goroshin, M. J. Soo, P. Julien, J. Palecka, D. L. Frost, D. J. Jarvis, Direct combustion of recyclable metal fuels for zero-carbon heat and power, Appl. Energ. 160 (2015) 368–382.

[3] P. Julien, J. M. Bergthorson, Enabling the metal fuel economy: green recycling of metal fuels, Sustain. Energy Fuels 1 (2017) 615–625.

[4] P. T. Lynch, High temperature spectroscopic measurements of aluminum combustion in a heterogeneous shock tube, Ph.D. thesis, University of Illinois at Urbana-Champaign (2010).

[5] T. Bazyn, H. Krier, N. Glumac, Evidence for the transition from the diffusion-limit in aluminum particle combustion, Proc. Combust. Inst. 31 (2007) 2021–2028.

[6] M. Marion, C. Chauveau, I. Gökalp, Studies on the ignition and burning of levitated aluminum particles, Combust. Sci. Technol. 115 (1996) 369–390.

[7] A. Braconnier, C. Chauveau, F. Halter, S. Gallier, Detailed analysis of combustion process of a single aluminum particle in air using an improved experimental approach, Int. J. Energ. Mat. Chem. Prop. 17 (2018) 111–124.

[8] C. K. Law, A simplified theoretical model for the vapor-phase combustion of metal particles, Combust. Sci. Technol. 7 (1973) 197–212.

[9] H. Yang, W. Yoon, Modeling of aluminum particle combustion with emphasis on the oxide effects and variable transport properties, J. Mech. Sci. Technol. 24 (2010) 909–921.

[10] P. Julien, M. Soo, S. Goroshin, D. L. Frost, J. M. Bergthorson, N. Glumac, F. Zhang, Combustion of aluminum suspensions in hydrocarbon flame products, J. Propuls. Power 30 (2014) 1047–1054.

[11] S. Mohan, M. A. Trunov, E. L. Dreizin, On possibility of vapor-phase combustion for fine aluminum particles, Combust. Flame 156 (2009) 2213–2216.

[12] B. T. Bojko, P. E. DesJardin, E. B. Washburn, On modeling the diffusion to kinetically controlled burning limits of micron-sized aluminum particles, Combust. Flame 161 (2014) 3211–3221.

[13] R. Lomba, P. Laboureur, C. Dumand, C. Chauveau, F. Halter, Determination of aluminum-air burning velocities using PIV and laser sheet tomography, Proc. Combust. Inst. 37 (2019) 3143–3150.

[14] Y. L. Shoshin, I. S. Altman, Integral radiation energy loss during single Mg particle combustion, Combust. Sci. Technol. 174 (2002) 209–219.

[15] J. Harrison, M. Q. Brewster, Analysis of thermal radiation from burning aluminium in solid propellants, Combust. Theor. Model. 13 (2009) 389–411.

[16] S. Goroshin, J. Mamen, A. Higgins, T. Bazyn, N. Glumac, H. Krier, Emission spectroscopy of flame fronts in aluminum suspensions, Proc. Combust. Inst. 31 (2007) 2011–2019.

[17] J. Kalman, T. Hedman, On the origin and use of the emissivity approximations for alumina particles, Propell. Explos. Pyrot. 41 (2016) 793–797.

[18] V. K. Bityukov, V. A. Petrov, Absorption coefficient of molten aluminum oxide in semitransparent spectral range, Appl. Phys. Res. 5 (2013) 51.

[19] E. L. Dreizin, On the mechanism of asymmetric aluminum particle combustion, Combust. Flame 117 (1999) 841–850.

[20] P. Julien, J. Vickery, S. Whiteley, A. Wright, S. Goroshin, J. M. Bergthorson, D. L. Frost, Effect of scale on freely propagating flames in aluminum dust clouds, J. Loss Prev. Process Ind. 36 (2015) 230–236.

[21] M. Soo, S. Goroshin, N. Glumac, K. Kumashiro, J. Vickery, D. L. Frost, J. M. Bergthorson, Emission and laser absorption spectroscopy of flat flames in aluminum suspensions, Combust. Flame 180 (2017) 230–238.

[22] N. A. Bergman, S. Chakraborty, Accidental fires and radiation heat transfer: Investigating the effects of flame impingement on structures, J. Purdue Undergrad. Res. 3 (2013) 16–23.

[23] D. W. Mackowski, R. A. Altenkirch, M. P. Menguc, A comparison of electromagnetic wave and radiative transfer equation analyses of a coal particle surrounded by a soot cloud, Combust. Flame 76 (1989) 415–420.

[24] D. W. Mackowski, R. A. Altenkirch, M. P. Menguc, Internal absorption cross sections in a stratified sphere, Appl. Opt. 29 (1990) 1551–1559.

[25] J. C. M. Garnett, XII. Colours in metal glasses and in metallic films, Philos. Trans. R. Soc. London, Ser. A 203 (1904) 385–420.

[26] Z. Hashin, S. Shtrikman, A variational approach to the theory of the effective magnetic permeability of multiphase materials, J. Appl. Phys. 33 (1962) 3125–3131.

[27] J. Y. Li, Q. Li, S. K. Dong, H. P. Tan, Radiative properties of radially non-isothermal alumina particles with multiphase, J. Quant. Spectrosc. Radiat. Transfer 113 (2012) 318–324.

[28] B. Hüttner, Optical properties of polyvalent metals in the solid and liquid state: aluminium, J. Phys.: Condens. Matter 6 (1994) 2459–2474.

[29] V. Sarou-Kanian, J.-C. Rifflet, F. Millot, IR radiative properties of solid and liquid alumina: Effects of temperature and gaseous environment, Int. J. Thermophys. 26 (2005) 1263–1275.

[30] J. K. R. Weber, S. Krishnan, C. D. Anderson, P. C. Nordine, Spectral absorption coefficient of molten aluminum oxide from 0.385 to 0.780 μm, J. Am. Ceram. Soc. 78 (1995) 583–587.

[31] L. Dombrovsky, Near-infrared properties of droplets of aluminum oxide melt, in: Thermopedia, Begel House Inc., 2011.

[32] L. Dombrovsky, Possibility of determining the dispersed composition of a two-phase flow from small-angle light scattering, High Temp. Sci. 20 (1982) 472–479.

[33] D. L. Parry, M. Q. Brewster, Optical constants of Al_2O_3 smoke in propellant flames, Journal of Thermophysics and Heat Transfer 5 (1991) 142–149.

[34] L. P. Bakhir, G. I. Levashenko, V. V. Tamanovich, Refinement of the imaginary part of the complex refractive index of liquid aluminum oxide, J. Appl. Spectrosc. 26 (1977) 378–383.

[35] I. H. Malitson, Refraction and dispersion of synthetic sapphire, J. Opt. Soc. Am. 52 (1962) 1377–1379.

[36] W. J. Wiscombe, Improved Mie scattering algorithms, Appl. Opt. 19 (1980) 1505–1509.

[37] A. Braconnier, Étude expérimentale de la combustion d'une particule d'aluminium isolée: influence de la pression et de la composition de l'atmosphère oxydante, Ph.D. thesis, Université d'Orléans (2020).

[38] Y. Plastinin, G. Karabdzhak, B. Khmelinin, G. Baula, A. Rodionov, Ultraviolet, visible and infrared spectra modeling for solid and liquid-fuel rocket exhausts, in: 39th Aerospace Sciences Meeting and Exhibit, American Institute of Aeronautics and Astronautics, 2001.

[39] J. Y. Yang, M. Xu, L. H. Liu, Infrared radiative properties of alumina up to the melting point: A first-principles study, J. Quant. Spectrosc. Radiat. Transfer 184 (2016) 111–117.

[40] N. Anfimov, G. Karabadyak, B. Khmelinin, Y. Plastinin, A. Rodionov, Analysis of mechanisms and the nature of radiation from aluminum oxide in different phase states in solid rocket exhaust plumes, in: 28th Thermophysics Conference, American Institute of Aeronautics and Astronautics, 1993.

[41] C. F. Bohren, D. R. Huffman, Absorption and scattering of light by small particles, John Wiley & Sons, New York, 1983.

[42] S. De Iuliis, R. Dondè, I. Altman, On pyrometry in particulate-generating flames, Combust. Sci. Technol. (2020) 1–15.

[43] T. Guerra, D. De Sousa Meneses, J.-P. Hugonin, C. Blanchard, Unconventional electromagnetic response of strongly coupled nanoparticles in the thermal infrared region: Link with effective medium properties and incoherent fields, Part. Part. Syst. Char. 39 (2022) 2100245.